Geotextiles and Geomembranes 42 (2014) 91–97

Contents lists available at ScienceDirect

Geotextiles and Geomembranes

journal homepage: www.elsevier.com/locate/geotexmem

Post-construction performance of a two-tiered geogrid reinforced soil wall backfilled with soil-rock mixture

Guang-Qing Yang [a,1], Huabei Liu [b,*], Yi-Tao Zhou [c,2], Bao-Lin Xiong [a,3]

[a] School of Civil Engineering, Shijiazhuang Tiedao University, Shijiazhuang 050043, China
[b] School of Civil Engineering and Mechanics, Huazhong University of Science and Technology, 1037 Luoyu Road, Wuhan, Hubei 430074, China
[c] Department of Transportation Engineering, Hebei Engineering and Technical College, Cangzhou 061001, China

ARTICLE INFO

Article history:
Received 3 June 2013
Received in revised form
13 January 2014
Accepted 27 January 2014
Available online 14 February 2014

Keywords:
Soil-rock mixtures
Two-tiered reinforced soil wall
Field instrumentation
Post-construction performance
HDPE geogrid

ABSTRACT

There have been very few studies on the application of soil-rock mixtures as the backfills of geogrid reinforced soil retaining walls with due concern for their long-term performance and safety. In this study, a 17-m high two-tiered reinforced soil wall backfilled with soil-rock mixture was instrumented for its performance under gravity load after construction. The instrumentation continued for 15 months. It is found that soil-rock mixtures with small rock content (<30%) have the potential to be used as the backfill materials of geogrid-reinforced retaining walls, but special attentions should be given to compaction quality, backfill–geogrid interaction, and installation damage to geogrids. Reinforcement slippage is possible because of the large particles, but it was small in this case and ceased to develop nine months after the end of construction. Compressibility difference between reinforced and unreinforced backfill might led to rotation of the upper tier. Using the estimated soil strength, the predictions of reinforcement loads by the FHWA methods were 100% higher than the estimated ones from measured strains.

1. Introduction

Use of locally-available geological materials as the backfills of geosynthetic reinforced soil retaining walls can further increase the cost-effectiveness of this type of earth structures, provided that the structure performance can be satisfactory. Since the emergence of geosynthetic reinforced soil technology, considerable efforts have been directed to test the feasibility of using different marginal backfill soils with cohesive contents or large percentage of non-plastic fines (e.g., Benjamim et al., 2007; Liu et al., 2009; Ling et al., 2012; Yang et al., 2012a), but very few studies have been reported on the application of soil-rock mixtures.

Soil-rock mixtures are commonly found geological materials in many places. According to many design guidelines of reinforced soil walls (e.g., Berg et al., 2009), if the materials are to be used as backfills, the rock content (particle size larger than 76.2 mm) should be removed, which considerably increases the construction cost. It is still not known if soil-rock mixtures with small rock content (<30%) can be used as the backfill materials of reinforced soil walls.

On another issue, there have been extensive full-scale test results on the performances of single-tiered reinforced soil walls (Allen and Bathurst, 2002; Benjamim et al., 2007; Bathurst et al., 2009; Kongkitkul et al., 2010; Yang et al., 2009, 2010; Horpibulsuk et al., 2011; Huang et al., 2013), but those of multi-tiered walls were still limited (Yoo and Jung, 2004; Yoo and Kim, 2008; Yoo et al., 2011; Stuedlein et al., 2012), although many high reinforced soil walls are now built in tiered configurations, and some analyses have shown that multi-tiered configuration may improve the performance of reinforced soil walls (Leshchinsky and Han, 2004).

In Shandong Province, China, a 17 m high two-tiered reinforced soil wall backfilled with soil-rock mixture was instrumented and monitored until 15 months after the end of construction. The soil-rock mixtures have a rock content of 15–25%. This study focuses on its post-construction performance, while its responses during construction were reported elsewhere (Yang et al., 2012b). It is hoped that the results from this field instrumentation will shed light on the application of soil-rock mixtures as backfill materials of reinforced soil walls. The results will also add to the literature of the full-scale test results of multi-tiered walls.

* Corresponding author. Tel.: +86 27 8755 7960; fax: +86 27 8754 2231.
E-mail addresses: gtsyang@163.com (G.-Q. Yang), hbliu@hust.edu.cn (H. Liu), zhouytwr@163.com (Y.-T. Zhou), xiongbao77@126.com (B.-L. Xiong).
[1] Tel.: +86 311 8793 6468.
[2] Tel.: +86 317 313 3169.
[3] Tel.: +86 311 8793 5535.

0266-1144/$ – see front matter © 2014 Elsevier Ltd. All rights reserved.
http://dx.doi.org/10.1016/j.geotexmem.2014.01.007

2. Field instrumentations

The two-tiered reinforced soil wall is located in Laiwu City in the middle of Shandong Province, China. It serves as a retaining wall of a large oxidized pellet facility in a steel plant. The hard-rock ground underneath the retaining wall has a very uneven surface; hence a concrete step-foundation was prepared before wall construction, as shown in Fig. 1. The wall is 17 m high, divided into a 7.9 m lower tier and a 9.1 m upper tier at an offset of 2 m. The total length of the wall is about 300 m. The modular block facings of both tiers were designed to have a 1:10 slope. The facing of the lower tier was directly placed on the concrete foundation without any fill in the front, as shown in Fig. 1. Construction of the retaining wall started in late March of 2010 and ended in early May of the same year. After the construction, no sizeable surcharge was applied on the backfill surface during the monitoring period.

Locally-available soil-rock mixtures were used as backfills in this project. The soil-rock mixtures were considerably heterogeneous, with a rock content (particle size $>$ 76.2 mm) ranging from 15% to 25% by weight. The largest particle size was larger than 20 cm. Excluding the rock content, the soil can be classified as poorly-graded gravel with sand according to United Soil Classification System. Fig. 2 shows a representative grain-size-distribution curve. The rock and gravel contents were weathered products of lime stone, while the rock particles are medium-weathered with visible cracks. The backfills were compacted using a heavy vibratory roller at a thickness of about 30 cm (after compaction), but the region 1.0 m away from the facing was densified by a lightweight vibrating rammer. Backfill compaction quality was monitored during the construction by water replacement method in a test pit (ASTM D5030-04, 2004), resulting in an average moist unit weight γ of 22.2 kN/m^3, but the backfill density varied considerably at different locations, and the dry unit weight γ_d ranged from 19.3 kN/m^3 to 21.4 kN/m^3. Due to the existence of large particles, the shear strength of the backfill was not directly tested. Instead, the design assumed a direct-shear friction angle ϕ of 35° without cohesion based on that of the soil content at medium dense state. According to limited studies on soil-rock mixtures, rock content could increase the friction angle of soil-rock mixtures by 1–5° when the rock content was in a range of 15–25% (Lindquist, 1994; Xu et al., 2011). Therefore, the actual angle of internal friction of the backfills, particularly the well-compacted portion, could be higher than what was used in the design.

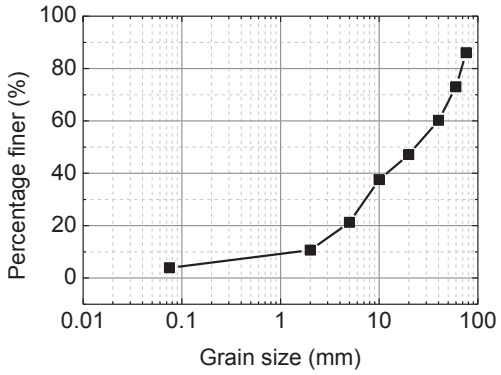

Fig. 2. Representative grain-size-distribution of the soil-rock mixtures.

Three types of HDPE geogrid were used as reinforcements. Fig. 3 shows the load–strain relationships of the geogrids at small strain using multi-rib tensile test as per ASTM D6637-11 (2011). Table 1 shows the strength and deformation properties of the geogrids. The creep strength was obtained as per ASTM D6992-03 (2003). 6 cm of HDPE geogrid was casted in the facing blocks, and connected to the geogrid reinforcement by bodkin joints. The reinforcement length was mainly 14 m in the lower tier and 10 m in the upper one. The reinforcement spacing was 0.3 m in the lower portion of the wall and 0.6 m in the upper portion, the details of which are shown in Fig. 1. The reinforcement layouts were determined as per the Chinese Standard (GB 50290-98, 1998), which satisfied the requirements of internal, external and compound stabilities.

The field instrumentations consist of the horizontal earth pressures at the back of the facings, the strains in selected reinforcement layers, and the lateral facing displacements at the toes and top of the wall. Vertical earth pressures in the backfills were also monitored, but there was relaxation below the pressure cells after certain fill heights, and the results afterwards were not reliable. The pressures and reinforcement strains were monitored during construction, but the lateral displacements were surveyed only after the end of construction. Fig. 1 shows the instrumentation layout. Among the instrumentations, the earth pressures were measured with vibrating-wire pressure cells, the measuring range of which is 0–600 kPa with a sensitivity of 1 kPa. The reinforcement

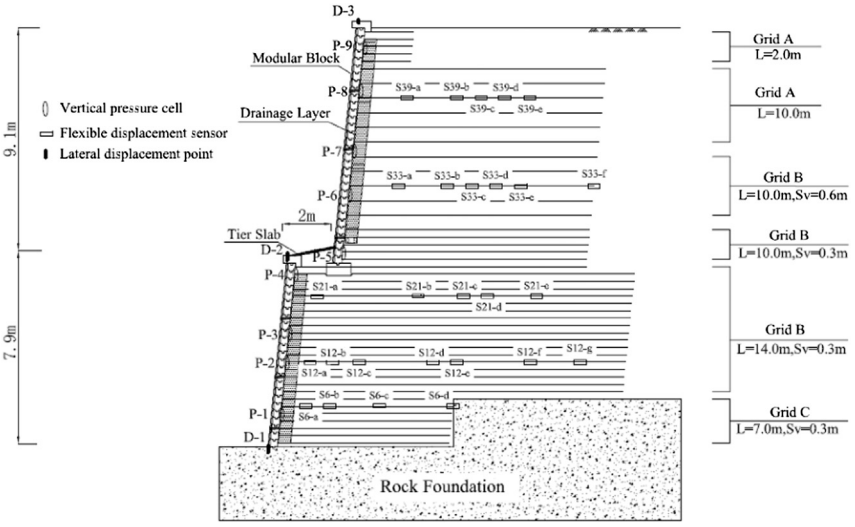

Fig. 1. Field instrumentation setup.

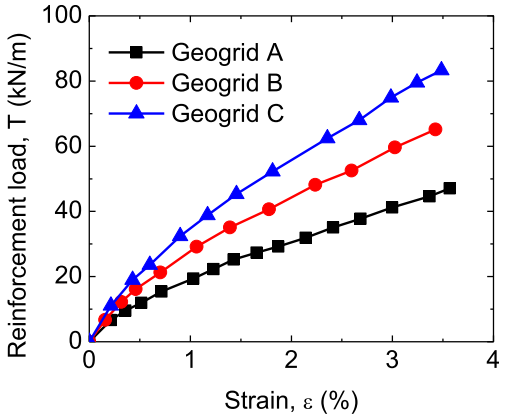

Fig. 3. Loads strain relationships of geogrids.

strain was measured by means of the inductive flexible displacement sensors, which were successfully tested in prior field tests (Yang et al., 2009, 2010 and 2012a). The maximum displacement of the sensors is 50 mm, corresponding to a maximum strain of 20% in this case. The sensitivity of the displacement sensor is 0.01 mm, corresponding to a strain of 0.004% in this case. The facing displacements after construction were measured by means of total station. Installation procedures of the earth pressure cells and inductive displacement sensors were introduced in details in Yang et al. (2009, 2010) and are not repeated herein to save space.

The monitoring period lasted 15 months after the end of construction, but the recording of some responses stopped earlier because of sensor malfunction. Overall, the instrumentation resulted in one year of complete data.

3. Results

3.1. Lateral earth pressure at the back of facing

Fig. 4 shows the lateral earth pressure distributions at the end of construction and post-construction. In the lower tier, the lateral earth pressure generally decreased after the end of construction, while in the upper tier, it decreased at the upper portion but increased at the lower portion. The decrease of lateral earth pressure with time was directly related to the increase of facing displacement with time, while the increase of lateral earth pressure at the lower portion of the upper tier was probably a result of rotation of the upper tier caused by differential settlement. It appears that the settlement at the rear of the lower tier was larger than that over the reinforced soil zone, which acted together with the shift of gravity centre to the back due to the tiered-configuration and caused the rotation of the upper tier. This rotation caused the larger earth pressure at the lower portion of the upper tier as well as the large post-construction lateral displacement at the mid-height of the wall (Yoo and Jung, 2004), as will be discussed in Section 3.4. The change of lateral earth pressure ceased to develop about one year after the end of construction.

Table 1
Properties of the geogrids.

	Geogrid A	Geogrid B	Geogrid C
Ultimate strength (kN/m)	90	130	170
Strength at 2% strain (kN/m)	23.7	38	52
Strength at 5% strain (kN/m)	45.2	75.5	102
Failure strain	8%	8%	8%
Creep strength at 120 years (kN/m)	34.9	50.4	55.9

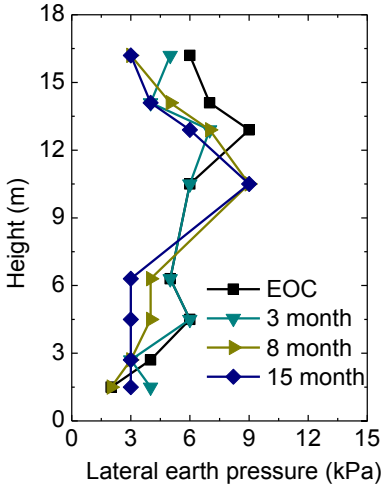

Fig. 4. Lateral earth pressures at the back of facing.

Overall the lateral earth pressure on the facing was small (<10 kPa), and it also did not increase with depth. Particularly close to the base of the lower tier, the lateral earth pressure was very small, possibly due to the sliding of facing base and the influence of the step foundation, which might have caused soil arching and reduced vertical soil stress at the wall base.

3.2. Reinforcement strains

Fig. 5 shows the reinforcement strain distributions at the end of construction. The surface of maximum reinforcement load predicted by the FHWA method (Berg et al., 2009) is also shown in Fig. 5. Overall the reinforcement strains were small (<0.5%), and they generally did not change considerably after the end of construction, as shown in Fig. 6. The number of inductive flexible displacement sensors in the legend of Fig. 6 can be found in Fig. 1. The strains of the lower reinforcement layers in both tiers increased slightly, and those of the upper layers decreased slightly or remained constant. There was also slight load redistribution in one reinforcement layer, as in the same layer, some location experienced slight increase of strain, while others experienced slight decrease. The increase of reinforcement strains was mainly the

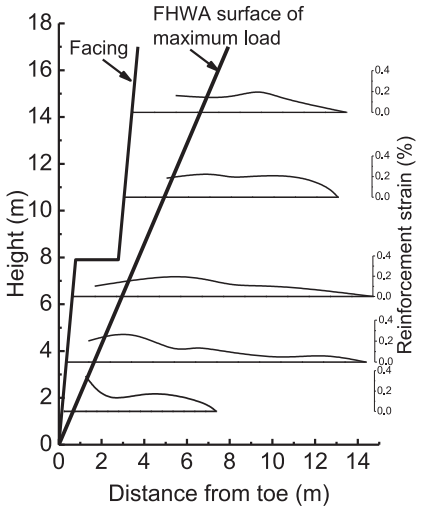

Fig. 5. Reinforcement strains at the end of construction.

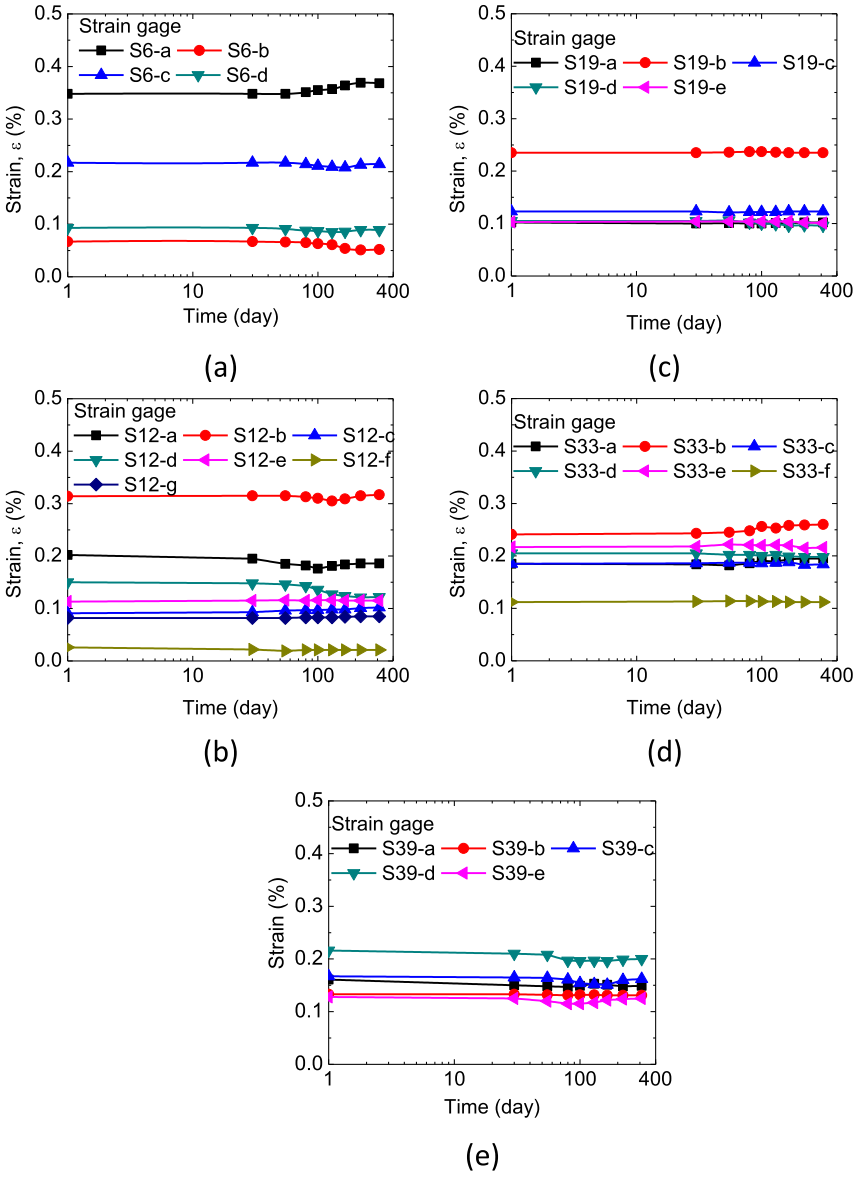

Fig. 6. Reinforcement strain variations after the end of construction: (a) 6th layer from bottom; (b) 12th layer from bottom; (c) 19th layer from bottom; (d) 33rd layer from bottom; (e) 39th layer from bottom.

result of time-dependent deformation of HDPE geogrid, which includes not only creep, but also stress relaxation and loading-rate effect (Helwany and Wu, 1995; Li and Rowe, 2008; Liu et al., 2009; Liu and Won, 2009; Liu, 2012). Compared to the prediction by the FHWA method, the location of maximum reinforcement load (strain) was farther away from the facing to some extent, but the difference was not large.

3.3. Reinforcement loads

Using the load–strain relationship of the geogrids and the reinforcement strains, the reinforcement loads in the wall can be interpreted. However, HDPE exhibits considerable time-dependent deformation under loading (Allen and Bathurst, 2002; Allen et al., 2003; Cholewa et al., 2011; Merry and Bray, 1997; Yeo and Hsuan, 2010), and its long term stiffness can be much smaller than the one obtained by standard uniaxial tension test. In addition, installation damage to the geogrid reinforcement (Lim and McCartney, 2013) may also reduce its long-term stiffness. Allen et al. (2003) and Bathurst et al. (2008) recommended a stiffness reduction factor of 25–35% for HDPE geogrid at 2% strain after 1000 h of creep or stress relaxation, but the strain in this study was much smaller (<0.5%), and the time-dependent deformation should also be smaller (Yeo and Hsuan, 2010). Very limited data are available on the long-term stiffness of HDPE geogrid at a strain smaller than 0.5%, but the test results on HDPE geomembrane (Merry and Bray, 1997) HDPE pipe materials (Cholewa et al., 2011) and HDPE rod (Bozorg-Haddad et al., 2010) showed that the stiffness of HDPE at around 0.5% strain after one to two months of creep was approximately 50% of the initial value. Since the wall construction was completed in about two months, this stiffness reduction factor was used in this study to interpolate the reinforcement loads at the end of construction. The reinforcement loads one year after the end of construction are not discussed herein due to the uncertainty on the reduction of reinforcement stiffness with time. Fig. 7 shows the estimated maximum reinforcement loads at the end of

construction in the instrumented layers. The estimated maximum reinforcement loads generally increased with depth. It should be pointed out that the reinforcement spacings of the top two layers in Fig. 7 were 0.6 m, instead of 0.3 m.

The maximum reinforcement loads predicted by the FHWA method (Berg et al., 2009) are also presented in Fig. 7. The plane-strain friction angle φ_{ps}, as estimated by $\varphi_{ps} = \tan^{-1}(1.2 \tan \varphi_{ds})$ (Allen et al., 2003), was used in this method. With a direct shear friction angle φ_{ds} of 35°, a plane strain friction angle φ_{ps} of 40° was obtained, which resulted in the reinforcement loads shown in Fig. 7. As can be seen in Fig. 7, the FHWA predictions of maximum reinforcement loads were more than 100% higher than the estimated ones based on the reinforcement strains. This difference cannot be explained by the possible underestimation of backfill strength and reinforcement stiffness. Neglecting facing restriction is one of the reasons for the conservatism (Bathurst et al., 2008; Leshchinsky et al., 2010; Ehrlich and Mirmoradi, 2013).

3.4. Later facing displacement after the end of construction

Lateral facing displacement was not monitored during construction, but no visible distress caused by large lateral facing displacement was observed during that period. The increase of facing displacement following the end of construction was surveyed using total station. Fig. 8 shows the displacement time-histories at the toe of the lower tier, at the top of the lower tier, and at the top of the upper tier. Four cross-sections that were 80 m apart were surveyed, and they yielded similar values of lateral displacement, as shown in Fig. 8. It can be seen that the post-construction displacement at the top of the lower tier was much higher than that of the upper tier. This trend was different from the post-construction lateral displacement of singled-tiered walls backfilled with granular soils (Liu et al., 2009; Kongkitkul et al., 2010; Liu, 2012). In that type of walls, the largest post-construction displacement occurred at the top of the walls. This difference is another proof that the upper tier rotated due to the shift of gravity centre and the difference of backfill compressibility. It is noted that similar response was observed by Yoo and Jung (2004) in their full-scale test. The lateral displacement ceased to develop approximately 9 months after the end of construction. This was also the time when the reinforcement strains ceased to change.

The post-construction displacement at the toe of the lower tier was also not negligible. It seems that the facing slid on the concrete foundation due to the lack of constraint in the front. This sliding has also led to the small lateral pressure at the back of facing (Fig. 4).

However, the post-construction lateral facing displacement was much higher than the integration of reinforcement strain increase. Three causes may have contributed to this discrepancy: a) the slag of reinforcement layer at its connection to the facing; b) the slippage of reinforcement layer with the backfill; and c) the lateral earth pressure at the back of the reinforced soil zone (Liu, 2012). It is not known which of these contributions was more important.

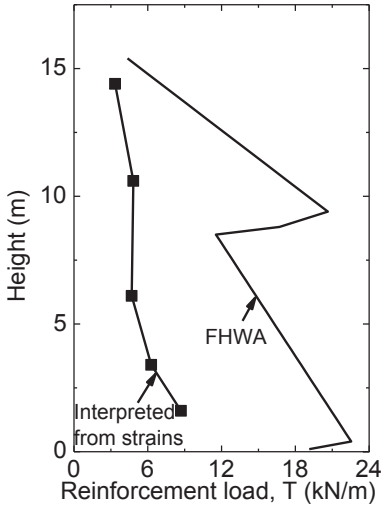

Fig. 7. Maximum reinforcement loads at the end of construction.

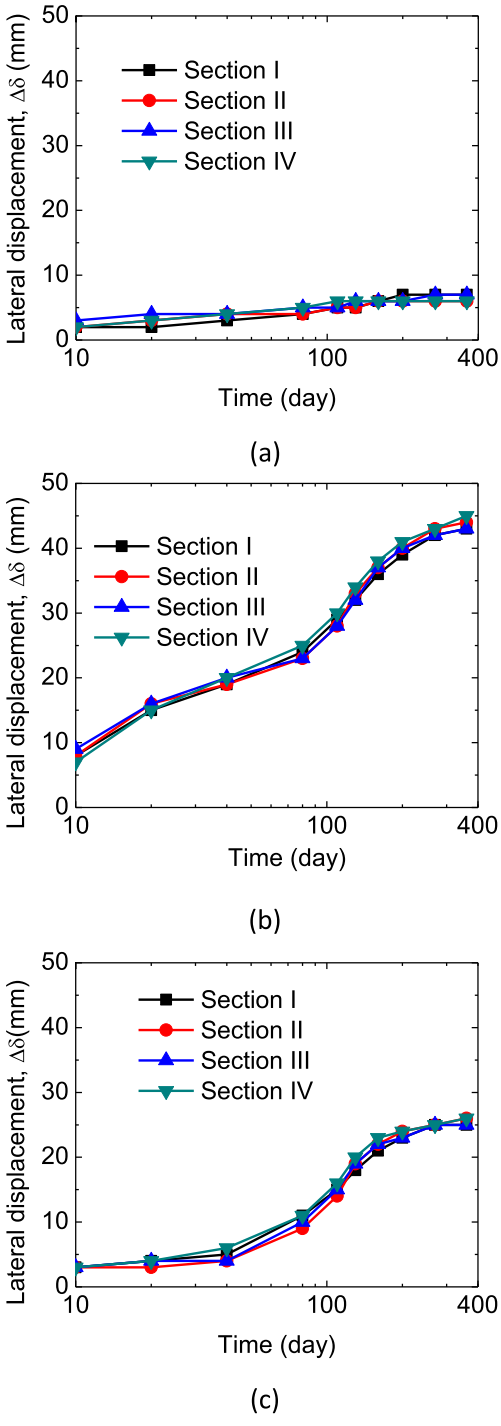

Fig. 8. Post-construction lateral facing displacement: (a) at the toe of the lower tier; (b) at the top of the lower tier; (c) at the top of the upper tier.

4. Discussions

Three important issues related to the application of soil-rock mixtures as backfill materials of reinforced soil walls can be identified from this field instrumentation: backfill compaction, geogrid–backfill interaction, and installation damage to the reinforcement.

In this wall, the backfill was compacted at a thickness of 30 cm (dense state). The loose thickness of fill layer was 35–40 cm. Some field study in China on the field compaction of soil-rock mixture has found that the loose thickness of fill should be at least 3 times larger than the maximum particle size (Xu et al., 2010), while the soil-rock mixture of this study had a maximum particle size that was larger than 20 cm, and it was also very heterogeneous. The fill thickness and the heterogeneous soil-rock mixture may have resulted in the large variability in the compacted backfill density, which may have also contributed to the differential settlement of the lower tier.

The aperture size of geogrid in this study was 2 cm × 25 cm. The interaction of this type of geogrid with sandy soil would have been good, but the existence of rock content may have significantly reduced the bonding strength between geogrid and backfill in localized regions. The small bonding strength, although localized, could have led to the reinforcement slippage as previously discussed.

Installation damage to the geogrid reinforcement caused by the soil-rock mixtures could be more significant than that by general granular soils (Bathurst et al., 2011; Lim and McCartney, 2013). This additional damage would reduce the long-term strength and stiffness of the backfill materials and should raise attention in the design and construction of this type of reinforced soil retaining walls. Specifically in this case, the wall has been in service for more than 3 years without any distress, indicating that the installation damage was not detrimental.

Another issue that deserves attention is the lateral displacement during construction. The localized small bonding between soil-rock mixtures and geogrid reinforcements might have caused additional compaction-induced lateral facing displacement (Ehrlich et al., 2012). Unfortunately the displacement was not measured, but it was believed to be non-destructive, since no sizable distress was observed during construction.

5. Conclusions

A high two-tiered reinforced soil wall backfilled with soil-rock mixture was instrumented for its post-construction performance for 15 months. The following conclusions can be obtained from this study:

a) When employing soil-rock mixtures as the backfill materials of geogrid-reinforced soil retaining walls, special attention should be given to the fill compaction quality, backfill–geogrid interaction, and installation damage to geogrid. The large particles in the backfill may significantly reduce the bonding strength between backfill and geogrid in localized regions.
b) The post-construction displacement of the reinforced soil wall was small (<0.3% H) and it ceased to develop approximately 9 months after the end of construction. Reinforcement slag, backfill-reinforcement slippage, and time-dependent properties of reinforced soil may have contributed to the post-construction lateral displacement.
c) The upper tier in a two-tiered reinforced soil wall may rotate towards to the back of the reinforcement, probably caused by differential settlement in the lower tier.
d) The estimations of maximum reinforcement loads by the FHWA design guidelines (Berg et al., 2009) were much higher than the measured ones, probably due to the neglecting of facing restriction.

Acknowledgement

The study was partly supported by the National Natural Science Foundation of China (Grant No. 51178280 and 51379082). Another support was from the Hebei Province Science and Technology Plan (Grant No. 11215612D). These supports are gratefully acknowledged.

References

Allen, T.M., Bathurst, R.J., 2002. Observed long-term performance of geosynthetic walls, and implications for design. Geosynth. Int. 9 (5–6), 567–606.
Allen, T.M., Bathurst, R.J., Holtz, R.D., Walters, D., Lee, W.F., 2003. A new working stress method for prediction of reinforcement loads in geosynthetic walls. Can. Geotech. J. 40 (5), 976–994.
ASTM D5030-04, 2004. Standard Test Method for Density of Soil and Rock in Place by the Water Replacement Method in a Test Pit. ASTM, West Conshohocken, Pennsylvania.
ASTM D6637-11, 2011. Standard Test Method for Determining Tensile Properties of Geogrids by the Single or Multi-Rib Tensile Method. ASTM, West Conshohocken, Pennsylvania.
ASTM D6992-03, 2003. Standard Test Method for Accelerated Tensile Creep and Creep-Rupture of Geosynthetic Materials Based on Time-Temperature Superposition Using the Stepped Isothermal Method. ASTM, West Conshohocken, Pennsylvania.
Bathurst, R.J., Miyata, Y., Nernheim, A., Allen, T.M., 2008. Refinement of K-stiffness method for geosynthetic reinforced soil walls. Geosynth. Int. 15 (4), 269–295.
Bathurst, R.J., Nernheim, A., Walters, D.L., Allen, T.M., Burgess, P., Saunders, D.D., 2009. Influence of reinforcement stiffness and compaction on the performance of four geosynthetic-reinforced soil walls. Geosynth. Int. 16 (1), 43–59.
Bathurst, R.J., Huang, B., Allen, T.M., 2011. Analysis of installation damage tests for LRFD calibration of reinforced soil structures. Geotext. Geomemb. 29, 323–334.
Benjamim, C.V.S., Bueno, B.S., Zornberg, J.G., 2007. Field monitoring evaluation of geotextile-reinforced soil-retaining walls. Geosynth. Int. 14 (2), 100–118.
Berg, R.R., Christopher, B.R., Samtani, N.C., 2009. Design and Construction of Mechanically Stabilized Earth Walls and Reinforced Slopes. No. FHWA-NHI-10-024 Vol. I and NHI-10–025 Vol II. Federal Highway Administration, Washington DC.
Bozorg-Haddad, A., Iskander, M., Wang, H.L., 2010. Compressive creep of virgin HDPE using equivalent strain energy density method. J. Mater. Civ. Eng. ASCE 22 (12), 1270–1281.
Cholewa, J.A., Brachman, R.W.I., Moore, I.D., 2011. Axial stress-strain response of HDPE from whole pipes and coupons. J. Mater. Civ. Eng. 23 (10), 1377–1386.
Ehrlich, M., Mirmoradi, S.H., Saramago, R.P., 2012. Evaluation of the effect of compaction on the behavior of geosynthetic-reinforced soil walls. Geotext. Geomemb. 34, 108–115.
Ehrlich, M., Mirmoradi, S.H., 2013. Evaluation of the effects of facing stiffness and toe resistance on the behavior of GRS walls. Geotext. Geomemb. 40, 28–36.
GB 50290-98, 1998. Chinese Technical Standard for Applications of Geosynthetics. China Zhijian Publishing House, Beijing, China.
Helwany, M.B., Wu, J.T.H., 1995. A numerical model for analyzing long-term performance of geosynthetic-reinforced soil structures. Geosynth. Int. 2 (2), 429–453.
Horpibulsuk, S., Suksiripattanapong, C., Niramitkornburee, A., Chinkulkijniwat, A., Tangsutthinon, T., 2011. Performance of an earth wall stabilized with bearing reinforcements. Geotext. Geomemb. 29 (5), 514–524.
Huang, J., Han, J., Parsons, R.L., Pierson, M.C., 2013. Refined numerical modeling of a laterally-loaded drilled shaft in an MSE wall. Geotext. Geomemb. 37, 61–73.
Kongkitkul, W., Tatsuoka, F., Hirakawa, D., Sugimoto, T., Kawahata, S., Ito, M., 2010. Time histories of tensile force in geogrid arranged in two full-scale high walls. Geosynth. Int. 17 (1), 12–32.
Leshchinsky, D., Han, J., 2004. Geosynthetic reinforced multitiered walls. J. Geotech. Geoenviron. Eng. ASCE 130 (12), 1225–1235.
Leshchinsky, D., Zhu, F., Meehan, C.L., 2010. Required unfactored strength of geosynthetic in reinforced earth structures. J. Geotech. Geoenviron. Eng. ASCE 136 (2), 281–289.
Li, A.L., Rowe, R.K., 2008. Effects of viscous behaviour of geosynthetic reinforcement and foundation soils on embankment performance. Geotext. Geomemb. 26 (4), 317–334.
Lim, S.Y., McCartney, J.S., 2013. Evaluation of effect of backfill particle size on installation damage reduction factors for geogrids. Geosynth. Int. 20 (2), 62–72.
Lindquist, E.S., 1994. The Strength and Deformation Properties of Melange. Ph.D. Thesis. University of California, Berkeley.
Ling, H.I., Leshchinsky, D., Mohri, Y., Wang, J.P., 2012. Earthquake response of reinforced segmental retaining walls backfilled with substantial percentage of fines. J. Geotech. Geoenviron. Eng. 138 (8), 934–944.
Liu, H., Wang, X., Song, E., 2009. Long-term behavior of GRS retaining walls with marginal backfill soils. Geotext. Geomemb. 27 (4), 295–307.

Liu, H., Won, M.S., 2009. Long-term reinforcement load of geosynthetic-reinforced soil retaining walls. J. Geotech. Geoenviron. Eng. ASCE 135 (7), 875–889.
Liu, H., 2012. Long-term lateral displacement of geosynthetic-reinforced soil segmental retaining walls. Geotext. Geomemb. 32, 18–27.
Merry, S.M., Bray, J.D., 1997. Time-dependent mechanical responses of HDPE geomembranes. J. Geotech. Geoenviron. Eng. ASCE 123 (1), 57–65.
Stuedlein, A.W., Allen, T.M., Holtz, R.D., Christopher, B.R., 2012. Assessment of reinforcement strains in very tall mechanically stabilized earth Walls. J. Geotech. Geoenviron. Eng. ASCE 138 (3), 345–356.
Xu, W.J., Xu, Q., Hu, R.L., 2011. Study on the shear strength of soil–rock mixture by large scale direct shear test. Int. J. Rock Mech. Min. Sci. 48, 1235–1247.
Xu, X.C., Zhou, W., Han, Z., Qin, S.L., Li, J.X., 2010. Research on compaction properties of soil-aggregate mixture. Rock Soil. Mech. 31 (Suppl. 2), 115–118 + 148 (in Chinese with English abstract).
Yang, G., Zhang, B., Lv, P., Zhou, Q., 2009. Behaviour of geogrid reinforced soil retaining wall with concrete-rigid facing. Geotext. Geomemb. 27 (5), 350–356.
Yang, G., Ding, J., Zhou, Q., Zhang, B., 2010. Field Behavior of a geogrid reinforced soil retaining wall with a wrap-around facing. Geotech. Test. J. 33 (1), 96–101.
Yang, G., Liu, H., Lv, P., Zhang, B., 2012a. Geogrid-reinforced lime-treated cohesive soil retaining wall: case study and implications. Geotext. Geomemb. 35, 112–118.
Yang, G.Q., Zhou, Y.T., Xiong, B.L., Liu, H.B., Dai, Z., 2012b. Behaviors of two-step geogrid reinforced earth retaining wall on rigid foundation. J. Hydraul. Eng. 43 (12), 1500–1506.
Yeo, S.S., Hsuan, Y.G., 2010. Evaluation of creep behavior of high density polyethylene and polyethylene-terephthalate geogrids. Geotext. Geomemb. 28 (5), 409–421.
Yoo, C., Jung, H.S., 2004. Measured behavior of a geosynthetic-reinforced segmental retaining wall in a tiered configuration. Geotext. Geomemb. 22 (5), 359–376.
Yoo, C., Kim, S.B., 2008. Performance of a two-tier geosynthetic reinforced segmental retaining wall under a surcharge load: full-scale load test and 3D finite element analysis. Geotext. Geomemb. 26 (6), 460–472.
Yoo, C., Jang, Y.S., Park, I.J., 2011. Internal stability of geosynthetic-reinforced soil walls in tiered configuration. Geosynth. Int. 18 (2), 74–83.